Speed-Sensorless Vector Torque Control of Induction Machines Using a Two-Time-Scale Approach

Heath Hofmann Seth R. Sanders
Department of Electrical Engineering and Computer Science
University of California, Berkeley

Abstract— After conditions for observability of a linearized induction machine model are examined, an approach for speed-sensorless flux estimation based on two-time-scale theory is developed. This approach relies on the natural time-scale separation between the electrical and mechanical dynamics of the induction machine. A full-order observer of an induction machine is presented, incorporating a correction term which has an intuitive explanation when one considers steady-state stator currents. Using two-time-scale theory, convergence of the observer is shown for all stable operating points of the induction machine with the exception of DC excitation. Sensitivity of the observer to parameter deviations is discussed. Experimental results are presented confirming the validity of the above approach.

I. Introduction

Many implementations of speed-sensorless flux estimation schemes are based on the so-called back-emf approach, which assumes a smooth-airgap model of an induction machine and requires measurements of only stator voltage and/or current. Several articles [1-5] present experimental data showing the effectiveness of these methods over a wide range of operating conditions. However, these articles do not consider the effect of operating point on convergence of the estimator in their stability analyses. For example, none of these methods can converge for DC excitation.

We propose an approach to speed-sensorless flux estimation using two-time-scale theory [6], which is based on the presumption that the electrical variables of an induction machine have significantly faster dynamics than the mechanical variables. As such, we can consider the electrical and mechanical dynamics separately, simplifying analysis. This approach for analyzing induction machine dynamics is discussed in [7]. We believe that two-time-scale theory is a natural approach for studying electrical machine systems.

We first discuss the conditions necessary for small-signal observability of an induction machine model using linear system theory. This presents a framework for discussing the limitations of any estimator based on the smooth-airgap model. We then develop a full-order observer of an induction machine. The observer incorporates a correction term which is injected into the observer subsystem corresponding to the mechanical dynamics. We use two-time-scale theory to show that the observer converges asymptotically for all stable steady-state operating points with the exception of DC excitation, provided the mechanical dynamics are slow compared to the electrical dynamics. We then analyze sensitivity of the observer to parameter deviations. Experimental data verifies the validity of the approach.

II. Induction Machine Model

The notation used throughout the paper is presented in Table I. We use a standard 2-axis smooth-airgap model for the induction machine, with stator current and rotor flux as the electrical state variables and rotor speed and load torque as the mechanical state variables.

$$\frac{d}{dt}\begin{bmatrix} \imath_s \\ \lambda_r \end{bmatrix} = \mathbf{A}_f(\dot{\rho},\omega_r)\begin{bmatrix} \imath_s \\ \lambda_r \end{bmatrix} + \begin{bmatrix} \frac{L_r}{\sigma^2} v_s \\ \mathbf{0} \end{bmatrix}, \tag{1}$$

$$\dot{\omega}_r = \frac{1}{H}(\tau_e - \tau_l - B\omega_r), \tag{2}$$

$$\dot{\tau}_l = 0, \tag{3}$$

$$\tau_e = \frac{M}{L_r} i_s^T \mathbf{J} \lambda_r, \tag{4}$$

$$\mathbf{A}_f(\dot{\rho},\omega_r) = \begin{bmatrix} -\frac{(R_s L_r^2 + R_r M^2)}{\sigma^2 L_r}\mathbf{I} - \dot{\rho}\mathbf{J} & \frac{M}{\sigma^2}\left(\frac{R_r}{L_r}\mathbf{I} - \omega_r \mathbf{J}\right) \\ \frac{R_r M}{L_r}\mathbf{I} & -\frac{R_r}{L_r}\mathbf{I} - (\dot{\rho} - \omega_r)\mathbf{J} \end{bmatrix}, \tag{5}$$

$$\mathbf{I} = \begin{bmatrix} 1 & 0 \\ 0 & 1 \end{bmatrix}, \mathbf{J} = \begin{bmatrix} 0 & -1 \\ 1 & 0 \end{bmatrix} \tag{6}$$

The variable ρ represents the angle corresponding to the chosen reference frame of the system. In the stationary

0-7803-3544-9/96 $5.00 © 1996 IEEE

Electrical Variables	
$\lambda_r = [\lambda_{rd}\ \lambda_{rq}]^T$	Rotor Flux Vector
$\imath_s = [\imath_{sd}\ \imath_{sq}]^T$	Stator Current Vector
$v_s = [v_{sd}\ v_{sq}]^T$	Stator Voltage Vector
ω_e	Electrical Frequency
Electrical Parameters	
$R_s = 1.59\Omega$	Stator Resistance
$R_r = 1.86\Omega$	Rotor Resistance
$L_s = 116.5mH$	Stator Inductance
$L_r = 116.7mH$	Rotor Inductance
$M = 109.5mH$	Mutual Inductance
$\sigma^2 = L_s L_r - M^2$	Leakage Term
$L_{\ell s} = L_s - M$	Stator Leakage Inductance
$L_{\ell r} = L_r - M$	Rotor Leakage Inductance
Mechanical Variables	
ω_r	Rotor Velocity
$\omega_s = \omega_e - \omega_r$	Slip Frequency
$\tau_e = \frac{M}{L_r} \imath_s^T \mathbf{J} \lambda_r$	Electromagnetic Torque
τ_ℓ	Load Torque
Mechanical Parameters	
$H = 0.8kg\,m^2$	Moment of Inertia of Rotor
$B = .1 \frac{kg\,m^2}{s}$	Damping Constant of Rotor

TABLE I
NOTATION

reference frame $\dot{\rho} = 0$, and in the electrical reference frame $\dot{\rho} = \omega_e$. We denote variables in the electrical reference frame with a superscript e (e.g., $\imath_s^e$). For the following analysis we choose the stator voltage as the reference vector in the electrical reference frame, hence $v_{sd}^e = \|v_s\|$ and $v_{sq}^e = 0$.

We denote steady-state electrical variables with a tilde (e.g., $\tilde{\imath}_s^e$). In electrical steady state we can write the stator current and rotor flux as a function of stator voltage, electrical frequency, and rotor speed.

$$\begin{bmatrix} \tilde{\imath}_s^e \\ \tilde{\lambda}_r^e \end{bmatrix} = -\mathbf{A}_f^{-1}(\omega_e, \omega_r) \begin{bmatrix} \frac{L_r}{\sigma^2} v_s^e \\ \mathbf{0} \end{bmatrix} \tag{7}$$

Note that we include mechanical dynamics in our model, where the machine load is modelled by a constant load torque term and a linear damping term. Although the assumption of constant load torque is made here and in the analysis of the observer, the experimental data show that the observer is also effective with other loads.

III. Observability of Induction Machine

We now analyze the conditions under which the model of the smooth-airgap induction machine is observable. First we note that the model is unobservable if the rotor flux is identically zero, because the rotor speed is introduced into the electrical dynamics through the back-emf $\lambda_r^e \omega_r$. However, we prove in [8] that in electrical steady-state the rotor flux is zero only in the trivial case of zero stator voltage excitation, and henceforth we assume $\tilde{\lambda}_r^e \neq \mathbf{0}$.

We study small-signal observability by linearizing the above induction machine model about an operating point and applying the concepts of observability from linear system theory [9]. Observability of the linearized system is the minimal requirement for exponential convergence of an observer. We study the system in the electrical reference frame; hence, the resulting linearized model will be time-invariant, although dependent upon operating point. The linearized induction machine dynamics are given by

$$\frac{d}{dt}\Delta x^e = \mathbf{A}_\ell(\tilde{\mathbf{x}}^e)\,\Delta x^e + \begin{bmatrix} \Delta v_s^e \\ \mathbf{0} \end{bmatrix}, \tag{8}$$

$$\Delta \imath_s^e = \mathbf{C}_\ell \Delta x^e, \tag{9}$$

$$\mathbf{A}_\ell(x^e) = \left[\begin{array}{cc|cc} & & \mathbf{0}_{2\times1} & \mathbf{0}_{2\times1} \\ \multicolumn{2}{c|}{\mathbf{A}_f(\omega_e,\omega_r)} & & \\ & & \mathbf{J}\lambda_r^e & \mathbf{0}_{2\times1} \\ \hline -\frac{M}{HL_r}\lambda_r^{eT}\mathbf{J} & \frac{M}{HL_r}\imath_s^{eT}\mathbf{J} & -\frac{B}{H} & -\frac{1}{H} \\ \hline \mathbf{0}_{1\times2} & \mathbf{0}_{1\times2} & 0 & 0 \end{array}\right], \tag{10}$$

$$x^e = \begin{bmatrix} \imath_s^e \\ \lambda_r^e \\ \omega_r \\ \tau_l \end{bmatrix}, \tag{11}$$

$$\mathbf{C}_\ell = [\ \mathbf{I}\ \ \mathbf{0}_{2\times4}\ ] \tag{12}$$

To test for observability we form the observability matrix:

$$\mathcal{C}_o = \begin{bmatrix} \mathbf{C}_\ell \\ \mathbf{C}_\ell\mathbf{A}_\ell \\ \mathbf{C}_\ell\mathbf{A}_\ell^2 \\ \mathbf{C}_\ell\mathbf{A}_\ell^3 \\ \mathbf{C}_\ell\mathbf{A}_\ell^4 \\ \mathbf{C}_\ell\mathbf{A}_\ell^5 \end{bmatrix} \tag{13}$$

The observability matrix $\mathcal{C}_o$ for the linearized induction machine model in variable form is too large to be included

in this paper (the matrix was generated using the analytical software MAPLE). We refer the interested reader to [8]. The linearized system is observable if and only if there is no vector $a \neq \mathbf{0}$ that satisfies

$$\mathcal{C}_o a = \mathbf{0}. \tag{14}$$

As shown in [8], the vector

$$a = \begin{bmatrix} \mathbf{0}_{2\times 1} \\ \left(\frac{R_r}{L_r}\mathbf{I} - \omega_r \mathbf{J}\right)^{-1} \mathbf{J}\lambda_r^e \\ 1 \\ -B - \frac{M}{R_r^2+\omega_r^2 L_r^2}\left[\imath_s^{e\,T}\left(R_r\mathbf{I} + \omega_r L_r \mathbf{J}\right)\lambda_r^e\right] \end{bmatrix} \tag{15}$$

is the only vector that can satisfy (14), and does so only if the electrical frequency ω_e is zero. Hence the smooth-airgap induction machine model is locally observable everywhere except for DC excitation.

IV. Two-Time Scale Approach to Observer Design

We denote observer variables with a hat (e.g., $\hat{\imath}_s$). The full-order observer is given by

$$\frac{d}{dt}\begin{bmatrix} \hat{\imath}_s \\ \hat{\lambda}_r \end{bmatrix} = \mathbf{A}_f(\hat{\rho}, \hat{\omega}_r)\begin{bmatrix} \hat{\imath}_s \\ \hat{\lambda}_r \end{bmatrix} + \begin{bmatrix} \frac{L_r}{\sigma^2} v_s \\ \mathbf{0} \end{bmatrix}, \tag{16}$$

$$\dot{\hat{\omega}}_r = \frac{1}{H}\left\{\hat{\tau}_e - \hat{\tau}_\ell - B\hat{\omega}_r - K_\omega f_{cx}\left(\imath_s, \hat{\imath}_s, v_s^e, \omega_e\right)\right\}, \tag{17}$$

$$\dot{\hat{\tau}}_\ell = K_\tau f_{cx}\left(\imath_s, \hat{\imath}_s, v_s^e, \omega_e\right), \tag{18}$$

$$\hat{\tau}_e = \frac{M}{L_r}\hat{\imath}_s^T \mathbf{J}\hat{\lambda}_r, \tag{19}$$

where $f_{cx}\left(\imath_s, \hat{\imath}_s, v_s^e, \omega_e\right)$ is an injection term designed to correct the mechanical dynamics of the observer.

We denote the error between observer and machine variables using the convention $\delta x = \hat{x} - x$. The nonlinear error dynamics are then given by

$$\frac{d}{dt}\begin{bmatrix} \delta\imath_s \\ \delta\lambda_r \end{bmatrix} = \mathbf{A}_f(\hat{\rho}, \omega_r)\begin{bmatrix} \delta\imath_s \\ \delta\lambda_r \end{bmatrix} + \begin{bmatrix} -\frac{M}{\sigma^2}\mathbf{J}\hat{\lambda}_r \\ \mathbf{J}\hat{\lambda}_r \end{bmatrix}\delta\omega_r, \tag{20}$$

$$\frac{d\left(\delta\omega_r\right)}{dt} = \frac{1}{H}\left\{\delta\tau_e - \delta\tau_\ell - B\delta\omega_r - K_\omega f_{cx}\left(\imath_s, \hat{\imath}_s, v_s^e, \omega_e\right)\right\}, \tag{21}$$

$$\frac{d\left(\delta\tau_\ell\right)}{dt} = K_\tau f_{cx}\left(\imath_s, \hat{\imath}_s, v_s^e, \omega_e\right) \tag{22}$$

We now consider convergence of the observer. The following analysis is limited to small-signal error dynamics of the observer about a steady-state operating point. Although small-signal stability is a minimal requirement, experiments characterizing the response of the observer show that it also works under transient condtions.

We prove convergence of the observer using two-time-scale theory [6]. With this approach we assume that the electrical error dynamics (20) are significantly faster than the mechanical error dynamics (21, 22). Hence when analyzing the electrical error dynamics one can assume that the rotor speed error is essentially constant. Analysis presented in [10] reveals that for any electrical frequency ω_e and rotor speed ω_r the matrix $\mathbf{A}_f\left(\omega_e, \omega_r\right)$ is exponentially stable. Hence the electrical error dynamics converge to a quasi-steady-state value which is a function of the rotor speed error.

$$\begin{bmatrix} \delta\tilde{\imath}_s^e \\ \delta\tilde{\lambda}_r^e \end{bmatrix} = -\mathbf{A}_f^{-1}(\omega_e, \omega_r)\begin{bmatrix} -\frac{M}{\sigma^2}\mathbf{J} \\ \mathbf{J} \end{bmatrix}\tilde{\lambda}_r^e \delta\omega_r + O\left(\delta\omega_r^2\right) \tag{23}$$

We now analyze the "slow" mechanical error dynamics separately, with the view that the fast electrical dynamics have converged to the quasi-steady-state given in (23). For example, we consider the electromagnetic torque error $\delta\tau_e$ to have reached a steady-state value $\delta\tilde{\tau}_e$. Using (7) and (23), we can write $\delta\tilde{\tau}_e$ as a function of the operating point of the machine (as characterized by v_s^e, ω_e, and ω_r), and the rotor speed error $\delta\omega_r$.

$$\begin{aligned} \delta\tilde{\tau}_e &= \frac{M}{L_r}\left(\tilde{\imath}_s^{e\,T}\mathbf{J}\tilde{\lambda}_r^e - \tilde{\imath}_s^{e\,T}\mathbf{J}\tilde{\lambda}_r^e\right) \\ &= \frac{M}{L_r}\left(\delta\tilde{\imath}_s^{e\,T}\mathbf{J}\delta\tilde{\lambda}_r^e + \delta\tilde{\imath}_s^{e\,T}\mathbf{J}\tilde{\lambda}_r^e + \tilde{\imath}_s^{e\,T}\mathbf{J}\delta\tilde{\lambda}_r^e\right) \\ &= g_\tau\left(v_s^e, \omega_e, \omega_r\right)\delta\omega_r + O\left(\delta\omega_r^2\right) \end{aligned} \tag{24}$$

The linear coefficient $g_\tau\left(v_s^e, \omega_e, \omega_r\right)$ is equivalent to $\frac{\partial\tilde{\tau}_e}{\partial\omega_r}$, the slope of the steady-state torque-speed curve for open-loop voltage excitation as shown in Figure 1. We note for future reference that $g_\tau\left(v_s^e, \omega_e, \omega_r\right)$ is negative in the open-loop stable operating region of the induction machine.

We now discuss the correction term $f_{cx}\left(\imath_s, \hat{\imath}_s, v_s^e, \omega_e\right)$. The formulation of this term can be understood by considering the locus of steady-state stator currents as a function of rotor speed, as shown in Figure 2. From Figure 2 it is evident that one can uniquely relate the steady-state stator current vector to the rotor speed. Furthermore, for a given stator voltage and excitation frequency both $\imath_s^e$ and $\hat{\imath}_s^e$ will be on the the same locus, with their positions depending on ω_r and $\hat{\omega}_r$, respectively. In order to develop the correction term we create the vectors $\imath_s^e - \imath_{sx}$ and $\hat{\imath}_s^e - \imath_{sx}$, such as those shown in Figures 3 and 4, where $\imath_{sx}$ is a vector in the stator current direct-quadrature plane whose coordinates are geometrically enclosed in the arc formed by the stator current locus. There is a monotonic dependence between the angle θ between these two vectors and the rotor speed error. Instead of calculating θ,

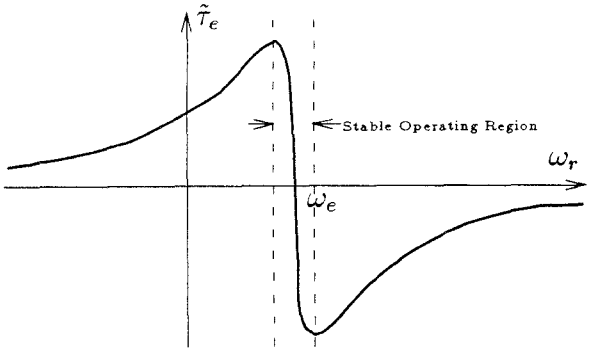

Fig. 1. Torque-speed curve

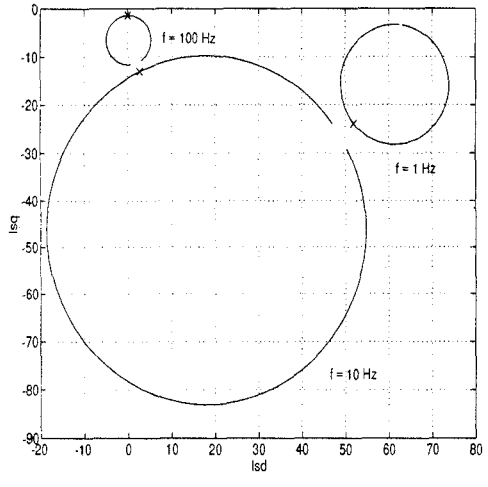

Fig. 2. Stator current locus in electrical reference frame aligned with the stator voltage as a function of rotor speed for various electrical frequencies, $v_{sd} = 100V$, and typical motor parameters. The 'x' corresponds to zero slip frequency.

however, we use the cross product of the two vectors as our correction term.

$$\begin{aligned} f_{cx}\left(\imath_s, \hat{\imath}_s, v_s^e, \omega_e\right) &= \left(\imath_s^e - \imath_{sx}\right)^T \mathbf{J}\left(\hat{\imath}_s^e - \imath_{sx}\right) \\ &= \left\|\imath_s^e - \imath_{sx}\right\| \left\|\hat{\imath}_s^e - \imath_{sx}\right\| \sin\theta \end{aligned} \quad (25)$$

Provided $\theta < 180°$, $f_{cx}\left(\tilde{\imath}_s, \tilde{\hat{\imath}}_s, v_s^e, \omega_e\right)$ has the same sign as θ, and therefore the same sign as the rotor speed error $\delta\omega_r$. Hence $f_{cx}\left(\tilde{\imath}_s, \tilde{\hat{\imath}}_s, v_s^e, \omega_e\right)$ can be used to correct estimated rotor speed.

We examine two particular choices for $\imath_{sx}$. One choice, $\imath_{sc}$, corresponds to the geometric center of the locus, as shown in Figure 3.

$$\imath_{sc} = \begin{bmatrix} \frac{R_s L_r}{R_s^2 L_r + L_s \sigma^2 \omega_e^2} \\ -\frac{\left(\sigma^2 + \frac{M^2}{2}\right)\omega_e}{R_s^2 L_r + L_s \sigma^2 \omega_e^2} \end{bmatrix} v_{sd}^e \quad (26)$$

The other choice, $\imath_{s\infty}$, corresponds to the theoretical steady-state stator current at infinite rotor speed, as shown in Figure 4.

$$\imath_{s\infty} = \left(R_s \mathbf{I} + \frac{\sigma^2}{L_r}\omega_e \mathbf{J}\right)^{-1} v_s^e \quad (27)$$

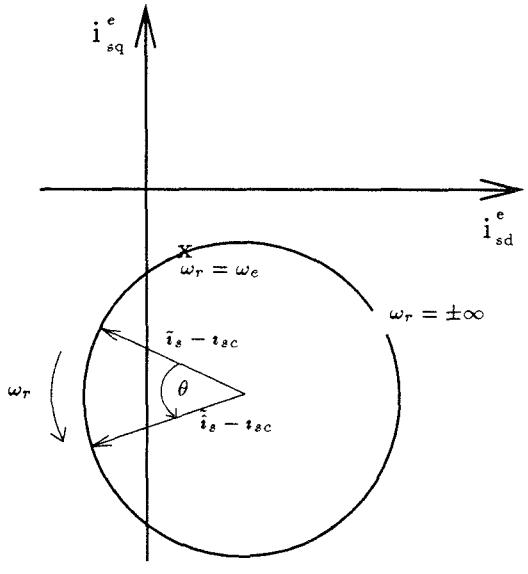

Fig. 3. Graphical description of correction term using coordinates corresponding to center of stator current locus

Both choices for $\imath_{sx}$ have features making them desirable. It is intuitively clear from Figures 4 and 3 that the choice of $\imath_{sc}$ will yield a greater sensitivity to the rotor speed error than $\imath_{s\infty}$. However, $\imath_{sc}$ has the disadvantage that for extremely large speed errors θ can become greater than 180°, in which case the sign of the cross product term differs from the sign of the rotor speed error. The vectors $\tilde{\imath}_s^e - \imath_{s\infty}$ and $\hat{\tilde{\imath}}_s^e - \imath_{s\infty}$ are never more than 180° apart, and so $f_{c\infty}\left(\tilde{\imath}_s, \tilde{\hat{\imath}}_s, v_s^e, \omega_e\right)$ is a valid correction term for all rotor speed errors.

In electrical steady-state, $f_{cx}\left(\tilde{\imath}_s, \tilde{\hat{\imath}}_s, v_s^e, \omega_e\right)$ can also be written as a function of the operating point and the speed error, using (7), (23), and the property $\boldsymbol{x}^T \mathbf{J} \boldsymbol{x} = 0$.

$$\begin{aligned} f_{cx}\left(\imath_s, \hat{\imath}_s, v_s^e, \omega_e\right) &= \left(\tilde{\imath}_s^e - \imath_{sx}\right)^T \mathbf{J}\left(\tilde{\hat{\imath}}_s^e - \imath_{sx}\right) \\ &= \left(\tilde{\imath}_s^e - \imath_{sx}\right)^T \mathbf{J}\left(\delta\tilde{\imath}_s + \tilde{\imath}_s^e - \imath_{sx}\right) \end{aligned}$$

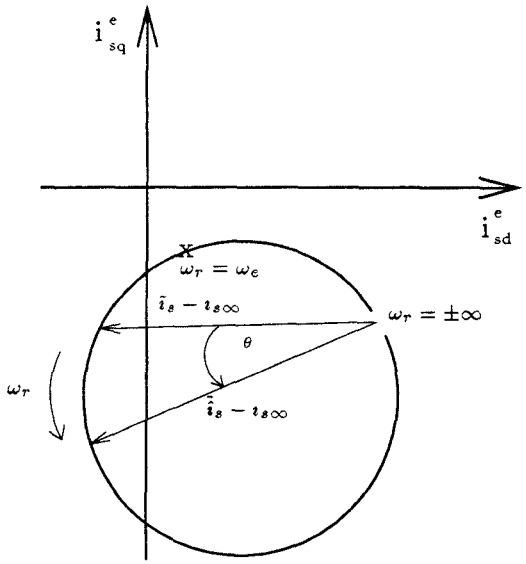

Fig. 4. Graphical description of correction term using coordinates corresponding to stator current at infinite rotor speed

$$= (\tilde{i}^e_s - \imath_{sx})^T \mathbf{J}\delta\tilde{i}_s$$
$$= h_{cx}(v^e_s, \omega_r, \omega_e)\,\delta\omega_r + O(\delta\omega_r^2) \quad (28)$$

As we are assuming small-signals, we neglect the higher-order terms of $\delta\omega_r$ and focus on the linear component $h_{cx}(v^e_s, \omega_r, \omega_e)\,\delta\omega_r$. Though not included in this paper, we show in [8] that $h_{cx}(v^e_s, \omega_r, \omega_e) > 0$ for all possible operating points with the exception of DC excitation. In the case of DC excitation the stator current locus collapses to a single point $\frac{v_s}{R_s}$, hence $i^e_s = \hat{i}^e_s = \imath_{sx}$ and the correction term vanishes. All speed estimation schemes that use only stator voltage and current measurements and assume the smooth-airgap model have this same limitation. That is, the stator current and voltage do not contain any information about the rotor speed at DC.

Figure 5 presents normalized 3-D plots of h_{cc}, $h_{c\infty}$, and g_τ for a range of operating points, characterized by the electrical and slip frequencies. Also shown is a contour plot of g_τ demarcating its regions of positive and negative sign.

Assuming that the electrical error dynamics have settled to their quasi-steady-state value, we can write the mechanical dynamics in linearized form

$$\begin{bmatrix} \delta\dot{\omega}_r \\ \delta\dot{\tau}_\ell \end{bmatrix} = \frac{1}{H}\mathbf{A}_s \begin{bmatrix} \delta\omega_r \\ \delta\tau_\ell \end{bmatrix}, \quad (29)$$

$$\mathbf{A}_s = \begin{bmatrix} (g_\tau - K_\omega h_{cx} - B) & -1 \\ HK_\tau h_{cx} & 0 \end{bmatrix} \quad (30)$$

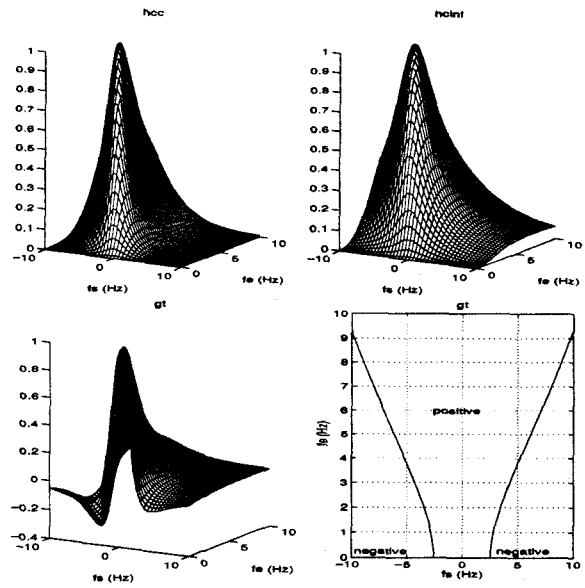

Fig. 5. Normalized 3-D plots of h_{cc}, $h_{c\infty}$, and g_τ as functions of electrical and slip frequency, with a contour plot of g_τ demarcating regions of positive and negative sign.

Provided the induction machine is operating in the stable operating range (i.e., $g_\tau(v^e_s, \omega_r, \omega_e) < 0$), it can be easily shown that the matrix $\mathbf{A}_s$ is exponentially stable if $h_{cx}(v^e_s, \omega_r, \omega_e) > 0$, stable if $h_{cx}(v^e_s, \omega_r, \omega_e) = 0$, and unstable if $h_{cx}(v^e_s, \omega_r, \omega_e) < 0$.

In the following we use the term $\frac{1}{H}$ to conceptually separate the time scales of the electrical and mechanical dynamics. In other words, provided the moment of inertia H is sufficiently large, the mechanical dynamics will be slow enough with respect to the electrical dynamics to validate the independent analysis.

We have now shown stability of both the fast and slow error dynamics. To prove stability of the entire system we use Corollary 3.1 of Kokotovic [6]. This corollary guarantees asymptotic stability of the error dynamics provided

- $\mathbf{A}_f$ and $\mathbf{A}_s$ are exponentially stable, and
- The "slow" dynamics are "slow" enough, i.e., $\frac{1}{H}$ is less than some upper bound ϵ.

The upper bound ϵ is difficult to determine. However, for a given steady-state operating point we can use (2.18) of Kokotovic to derive a lower bound for ϵ (see [8] for details).

$$\epsilon \geq \frac{1}{\|A_f^{-1}(\omega_e, \omega_r)\| \left[a + b + 2(ab)^{1/2}\right]}, \quad (31)$$

$$a = \|\mathbf{A}_s\|, \quad b = c\|\mathbf{A}_f^{-1}(\omega_e, \omega_r)\|\,\|\tilde{\lambda}^e_r\|, \quad (32)$$

$$c = \sqrt{\left(\frac{M}{L_r}\left\| \begin{bmatrix} \tilde{i}_s^e \\ \tilde{\lambda}_r^e \end{bmatrix} \right\| + K_\omega \|i_s^e - i_{sx}\|\right)^2 + H^2 K_\tau^2 \|i_s^e - i_{sx}\|^2} \tag{33}$$

This lower bound supports the intuition that there are upper limits to the choices of gains K_ω and K_τ that satisfy the assumptions of the two-time-scale theory. However, as (31) is only a lower bound for ϵ, it is desirable to determine the gains through simulation or experimentation in order to achieve satisfactory performance.

V. Parameter Sensitivity

This section analyzes the effect of errors in the observer parameters on the observer's performance. As many field-oriented torque-control schemes used in practice are rotor-flux-based, we analyze the effect of parameter deviation on the steady-state rotor flux angle and magnitude. Analysis is limited to operating points where the slip frequency is set to one-tenth the value of the electrical frequency. We first calculate $\tilde{\lambda}_r^e$ for a given operating point. We then alter a parameter in the observer model and calculate $\tilde{\tilde{\lambda}}_r$ such that $(\tilde{i}_s^e - i_{sx})^T \mathbf{J} (\tilde{i}_s^e - i_{sx}) = 0$ is satisfied. This corresponds to the condition when the observer has converged to its steady-state value.

Figures 6, 7, and 8 present angular and magnitude errors of the observer rotor flux due to deviations in the parameters R_s, M, and L_{ls}, respectively. The correction term makes the rotor flux completely insensitive to R_r and highly insensitive to L_{lr} in steady-state, and so sensitivity to these parameters is not presented in this paper. In this analysis we chose $i_{sx} = i_{sc}$. The sensitivity analysis for $i_{s\infty}$ is not presented, as it is similar to that of i_{sc}.

It is apparent from Figures 6, 7, and 8 that the observer is highly sensitive to deviations in R_s, M, and L_{ls} at low electrical frequencies. As stator resistance can vary markedly due to temperature, it is desirable to either include a temperature-compensated model for R_s or implement a stator resistance estimation scheme. The parameters L_{ls} and M can also vary due to magnetic saturation. However, we note that the above observer can readily incorporate a nonlinear magnetics model, such as the one presented in [11].

VI. Implementation

We implemented the observer on a 90MHz personal computer which samples stator voltages and currents and commands stator voltage values with sampling time $T_s = 100\mu s$. The computer numerically integrates (16), (17), and (18) using the third-order Adams-Bashforth method [12]. In order to generate the correction term $f_{cx}(i_s, \hat{i}_s, v_s^e, \omega_e)$, the computer must transform the motor

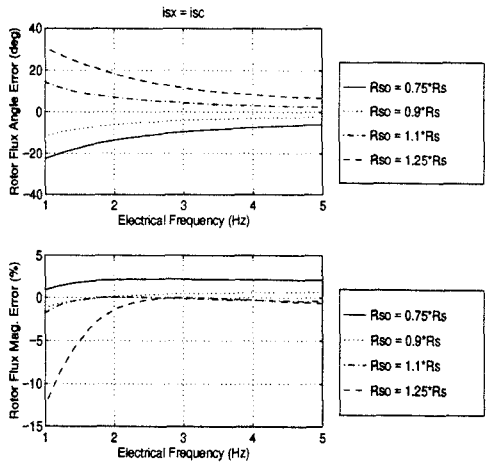

Fig. 6. Steady-state observer rotor flux error due to deviations in R_s using correction term $f_{cc}(i_s, \hat{i}_s, v_s^e, \omega_e)$, $\omega_s = \omega_e/10$

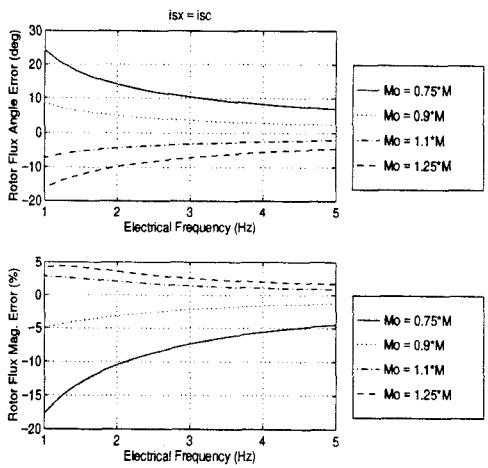

Fig. 7. Steady-state observer rotor flux error due to deviations in M using correction term $f_{cc}(i_s, \hat{i}_s, v_s^e, \omega_e)$, $\omega_s = \omega_e/10$

and observer stator currents into the electrical reference frame with respect to the stator voltage. This is done using the transformation

$$i_s^e = \frac{1}{\|v_s\|} \begin{bmatrix} v_{sd} & v_{sq} \\ -v_{sq} & v_{sd} \end{bmatrix} i_s \tag{34}$$

Knowledge of the electrical frequency is also necessary to determine $f_{cx}(i_s, \hat{i}_s, v_s^e, \omega_e)$. We calculate electrical frequency using a formula presented in [13].

$$\omega_e = \frac{\dot{v}_s^T \mathbf{J} v_s}{\|v_s\|^2}, \tag{35}$$

where $\dot{v}_s$ is calculated using a bandlimited numerical differentiation scheme.

We test the observer by implementing torque steps at low rotor speeds. Torque commands are generated through control of the direct and quadrature components

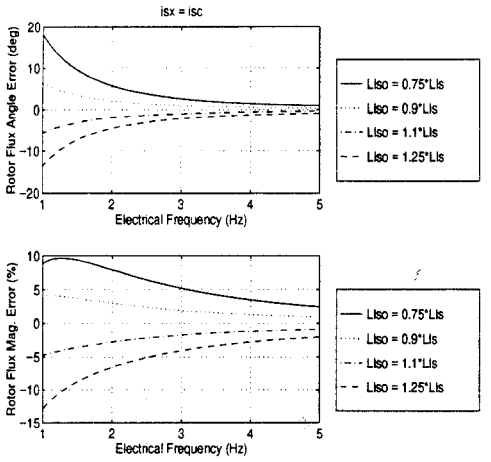

Fig. 8. Steady-state observer rotor flux error due to deviations in $L_{\ell s}$ using correction term $f_{cc}(\imath_s, \hat{\imath}_s, v_s^e, \omega_e)$, $\omega_s = \omega_e/10$

of stator flux in the rotor flux reference frame, as presented in [13]. Figures 9 and 10 show the result of torque step commands with a 40kW separately excited dynamometer providing resistive loading for the induction machine. Figure 11 shows the results of a locked rotor test, with a torque step from zero to rated torque. Although the rotor was locked, this information was not supplied to the observer. We estimate torque using the cross product of estimated stator flux and measured stator current, i.e., $3\hat{\lambda}_s^T \mathbf{J} \imath_s$. Also presented in the plots are estimated rotor speed and observer and motor stator currents in the electrical reference frame with respect to the rotor flux.

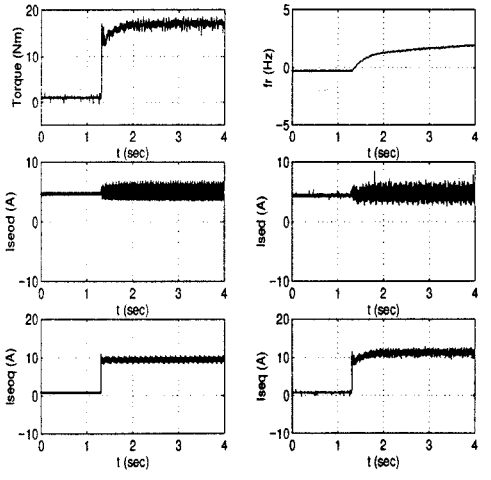

Fig. 9. Torque step from $0\,N \cdot m$ to $18\,N \cdot m$. Plots, going clockwise from the top left, are estimated torque, observer rotor speed, direct and quadrature motor stator current, and quadrature and direct observer stator current. Currents are displayed in the electrical reference frame with respect to rotor flux.

For these experiments we use the correction term $f_{cc}(\imath_s, \hat{\imath}_s, v_s^e, \omega_e)$. In order to reduce the effect of the induction machine operating point on the correction term, we choose variable gains $K_\omega = \frac{1000}{\|\imath_s^e - \imath_{sx}\|\|\hat{\imath}_s^e - \imath_{sx}\| + .001}$ and $K_\tau = \frac{1}{\|\imath_s^e - \imath_{sx}\|\|\hat{\imath}_s^e - \imath_{sx}\| + .001}$. If we neglect the small constant in the denominator, which is included to avoid a singularity at DC excitation, we have $K_\omega f_{cc}(\imath_s, \hat{\imath}_s, v_s) = 1000 \sin\theta$ and $K_\tau f_{cc}(\imath_s, \hat{\imath}_s, v_s) = \sin\theta$.

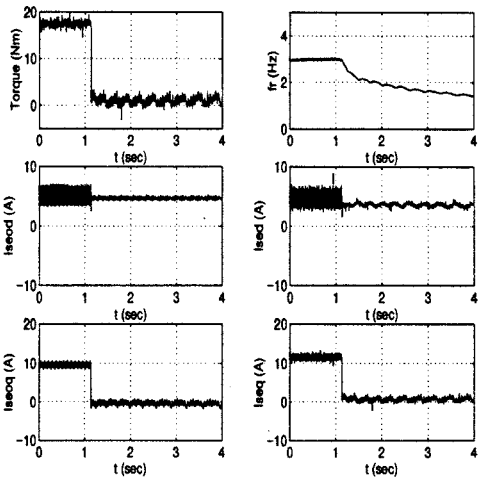

Fig. 10. Torque step from $18\,N \cdot m$ to $0\,N \cdot m$. Plots as in Figure 9.

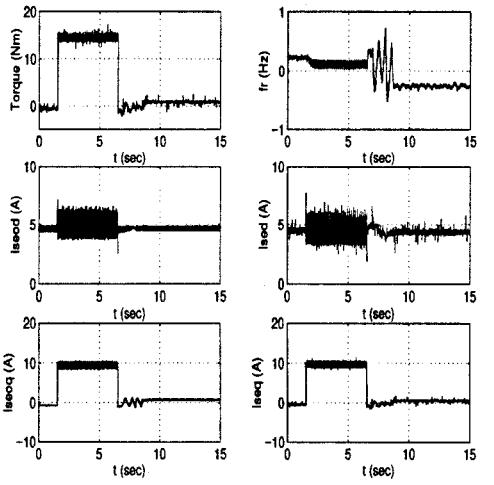

Fig. 11. Torque step from no torque to rated torque, locked rotor. Plots as in Figure 9.

The motor used in the experiments is a 3-phase, 4-pole wound rotor induction machine rated at 3 hp, 1800 rpm, and 220V line-to-line. The motor is driven by a commercial pulse-width-modulated (PWM) IGBT inverter rated at 36A and 460V. The microprocessor control provided in the inverter was replaced with custom hardware that directly accesses the gate drive modules. This hardware consists of a three phase 15kHz PWM modulator that interfaces with two-axis command voltages supplied by the personal computer. Hall-effect sensors within the inverter measure the stator current and 100:1 voltage probes measure the stator voltage.

VII. Analysis of Another Full-Order Observer

The two-time-scale approach can also be used to analyze other speed-sensorless control schemes. For example, we consider the full-order adaptive observer presented in [1]. This observer is a convenient choice for analysis, as it uses the same model for electrical dynamics presented in this paper (see (16)). Though reference [1] discusses the use of feedback injection into the electrical dynamics, this is not implemented in their experiments, and so we do not include this feedback injection in the following analysis.

For the mechanical dynamics, reference [1] assumes constant rotor speed, and estimates this speed using the following correction term:

$$\dot{\hat{\omega}}_r = -\hat{\lambda}_r^T \mathbf{J} \left(\hat{\imath}_s - \imath_s \right) \tag{36}$$

By assuming that the electrical error variables have converged to the quasi-steady-state of (23), we can write the rotor speed error dynamics in terms of the rotor speed error and the operating point of the machine (7).

$$\begin{aligned} \delta\dot{\omega}_r &= -\tilde{\hat{\lambda}}_r^{e\,T} \mathbf{J} \delta i_s^e \\ &= -h_{ck} \left(v_s, \omega_r, \omega_e \right) \delta\omega_r + O\left(\delta\omega_r^2 \right) \end{aligned} \tag{37}$$

Once again we assume small signals and therefore neglect the higher-order terms of (37). Based on the assumptions of two-time-scale theory, the rotor speed error dynamics are locally asymptotically stable if $h_{ck}\left(v_s^e, \omega_r, \omega_e \right) > 0$, and unstable if $h_{ck}\left(v_s^e, \omega_r, \omega_e \right) < 0$.

Figure 12 shows a normalized 3-D plot and contour plot of $h_{ck}\left(v_s^e, \omega_r, \omega_e \right)$ using the motor parameters presented in this paper. The contour plot of $g_\tau\left(v_s^e, \omega_r, \omega_e \right)$ is superimposed over h_{ck} for reference. Though $h_{ck}\left(v_s^e, \omega_r, \omega_e \right) > 0$

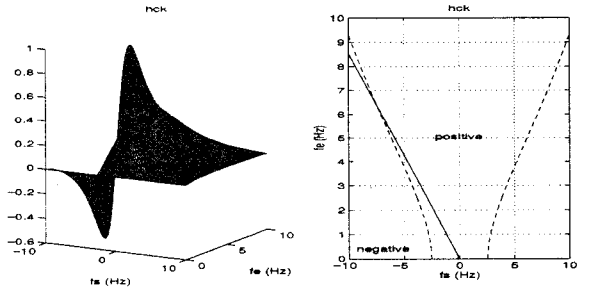

Fig. 12. Normalized 3-D plot of h_{ck} and contour plots of h_{ck} (solid line) and g_τ (dashed line) demarcating regions of positive and negative sign. Regions of positive and negative sign of h_{ck} are specified. Typical motor parameters.

for a wide range of operating conditions, there exists a range of operating points in the generating region ($\omega_s < 0$) where it becomes negative, and hence the observer does not converge under the assumptions of the two-time-scale theory. We note, however, that only a limited portion of this unstable range overlaps with the stable operating region of the induction machine, as shown in Figure 12.

VIII. Conclusion

We have shown two-time-scale theory to be an effective tool in the analysis of induction machine observers. Using the assumption of separate time scales, a full-order observer has been designed that converges at all operating points with the exception of DC excitation. Though the technique was used in this paper to estimate rotor speed, the same approach could be used to estimate other parameters of an induction machine that are slowly varying, such as stator resistance. Further study is warranted to explore the usefulness of this approach.

IX. Acknowledgements

This work has been supported by NSF Grant ECS-9358284. The authors would also like to thank Tzu-Yi Chen for her efforts in proofreading this manuscript.

References

[1] H. Kubota, K. Matsuse, and T. Nakano. DSP-based speed adaptive flux observer of induction motor. *IEEE Transactions on Industry Applications*, 29(2):344–348, March/April 1993.

[2] Y. Kim, S. Sul, and M. Park. Speed sensorless vector control of induction motor using extended kalman filter. *IEEE Transactions on Industry Applications*, 30(5):1225–1233, Sept./Oct. 1994.

[3] F. Peng and T. Fukao. Robust speed identification for speed-sensorless vector control of induction motors. *IEEE Transactions on Industry Applications*, 30(5):1234–1240, Sept./Oct. 1994.

[4] N. Rubin, R. Harley, and G. Diana. Evaluation of various slip estimation techniques for an induction machine operating under field-oriented control conditions. *IEEE Transactions on Industry Applications*, 28(6):1367–1375a, December 1992.

[5] H. Nakano and I. Takahashi. Sensorless field-oriented control of an induction motor using an instantaneous slip frequency estimation method. In *PESC '88 Record*, pages 847–854, 1988.

[6] P. Kokotovic, H. K. Khalil, and J. O'Reilly. *Singular Perturbation Methods in Control: Analysis and Design*. Academic Press, 1986.

[7] M. Velez-Reyes and G. Verghese. Developing reduced order electrical machine models using participation factors. *Modelling and Simulation of Systems*, 3(1):333–335, 1989.

[8] H. Hofmann. Vector torque control of induction machines. Master's thesis, The University of California at Berkeley, 1996.

[9] T. Kailath. *Linear Systems*. Prentice Hall, 1980.

[10] G. Verghese and S. Sanders. Observers for flux estimation in induction machines. *IEEE Transactions on Industrial Electronics*, 35(1):85–94, February 1988.

[11] C. R. Sullivan and S. R. Sanders. Models for induction machines with magnetic saturation of the main flux path. *IEEE Transactions on Industry Applications*, 31(4):907–17, July-August 1995.

[12] J. D. Lambert. *Numerical Methods for Ordinary Differential Systems: The Initial Value Problem*. John Wiley and Sons, 1991.

[13] C. Sullivan, C. Kao, B. Acker, and S. Sanders. Control systems for induction machines with magnetic saturation. *IEEE Transactions on Industrial Electronics*, 43(1), February 1996.